Video Images Fusion to Improve Iris Recognition Accuracy in Unconstrained Environments

Juan M. Colores-Vargas[1], Mireya García-Vázquez[1], Alejandro Ramírez-Acosta[2], Héctor Pérez-Meana[3], and Mariko Nakano - Miyatake[3]

[1] Instituto Politécnico Nacional, CITEDI
Avenida del Parque 1310, Tijuana, B.C. México 22510
[2] MIRAL R&D, Palm Garden, Imperial Beach, USA 91932
[3] Instituto Politécnico Nacional, ESIME-Culhuacan, DF., México
colores@citedi.mx, msarai@ipn.mx, ramacos10@hotmail.com,
{mnakano,hmperezm}@ipn.mx

Abstract. To date, research on the iris recognition systems are focused on the optimization and proposals of new stages for uncontrolled environment systems to improve the recognition rate levels. In this paper we propose to exploit the biometric information from video-iris, creating a fusioned normalized template through an image fusion technique. Indeed, this method merges the biometric features of a group of video images getting an enhanced image which therefore improves the recognition rates iris, in terms of Hamming distance, in an uncontrolled environment system. We analyzed seven different methods based on pixel-level and multi-resolution fusion techniques on a subset of images from the MBGC.v2 database. The experimental results show that the PCA method presents the best performance to improve recognition values according to the Hamming distances in 83% of the experiments.

Keywords: Fusion, Iris, MBGC, PCA, Recognition.

1 Introduction

To date, the commercial iris recognition systems based on still images [1-2] are designed to work with special or restricted conditions. This means that they require an ideal environment and cooperative user's behavior during the iris image acquisition stage to obtain high quality images. Therefore, if any of these requirements are not met, it can cause a substantially increase of error rates, specially the false rejections. Many factors can affect the quality of an iris image, including defocus, motion blur, dilation and heavy occlusion. Naturally, poor image's quality cannot generate satisfactory recognition because they do not have enough feature information, in this regard; iris recognition is dependent on the amount of information available in two iris images being compared. A typical iris recognition system commonly consists of four main modules as shown in Figure 1:

- **Acquisition** the aim is to acquire a high quality image.

J.A. Carrasco-Ochoa et al. (Eds.): MCPR 2013, LNCS 7914, pp. 114–125, 2013.

- **Preprocessing**, involves the segmentation and normalization processes. The segmentation consists in isolating the iris region from the eye image. The normalization is used to compensate the varying size of the pupil.
- **Feature encoding**, uses texture analysis method to extract features from the normalized iris image. The significant features of the iris are extracted as a series of binary codes known as digital biometric template.
- **Matching** compares the user digital biometric template with all the stored templates in the database. The matching metric will give a range of values of the compared templates from the same iris.

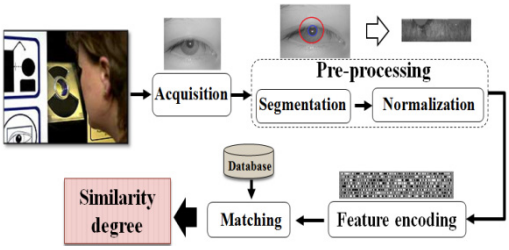

Fig. 1. Architecture for iris recognition system

In recent years, with an increasing of new massive biometric security demands around the world, it seems difficult to fulfill the conditions mentioned above in order to have a reliable iris recognition system [3-4]. Thus, with the aim of overcoming these drawbacks, news approaches are being developed in an attempt to improve iris recognition performance under non ideal situations. Among these approaches, the video-based eye image acquisition for iris recognition seems to be an interesting alternative [5-7] because it can provide more information through the capture of a video iris sequences. Besides that, it is a friendly system because it is not intrusive and requires few users' cooperation. In this paper, we propose to use the video-iris. It contains information related to the spatio-temporal activity of the iris and its neighbor region over a short period of time, such that, iris images can be selectively chosen for fusion while avoiding poor quality images. Therefore, the information from individual iris images can be fused into a single composite iris image with higher biometric information, resulting in better recognition performance and reducing the error rates.

The idea of fusing iris templates to perform biometric recognition has been recently described in the literature. Jillela and Ross [8] fused frames of iris videos using a variation of the PCA method with three data-level resolution, the performance of the image-level fusion was compared against that of score-level fusion, they observe significant improvements of the proposed technique, when compared to the use of any individual frame. Hollingsworth et al. [5] improve the matching performance using signal-level fusion. From multiple frames of iris video, they created a single average image, having observed that signal-level fusion performs comparably to state-of-the-art score-level fusion techniques. There are several methods of fusion, the main objective in this research is to experiment and analyze some fusion methods to determine the most suitable to be included as a step in the recognition system for unconstrained environments. This paper is organized as

follows: section 2 explains the basics of the evaluated image fusion methods. Section 3 presents the evaluation methodology and the evaluation results, finally in section 4 presents the conclusions and future work.

2 Image Fusion

The image fusion tries to solve the problem of combining information from several images taken the same object to get a new fusioned [9]. In this paper, each image of video is first pre-processed in order to obtain a single normalized template. Then, a fusion method is applied to provide a representative fusioned normalized template from these individual normalized templates. The resulting template should be contains more texture information as compared to individual templates. We analyzed the image fusion methods to determine the most suitable to achieve greater extraction of texture information. The image fusion methods can be categorized in two categories: pixel level and multi-resolution.

- **Pixel-level methods,** the input images are fused pixel by pixel followed by the information extraction. To implement the pixel level fusion, arithmetic operations are widely used, include basic arithmetic operations, logical operations and probabilistic operations.
- **Multi-resolution methods,** Multi-scale Transform (MST) is applied on the original images to construct a composite representation followed by down-sampling. Then an image fusion rule is applied to fuse the images in the MST format. After that, an Inverse Multi-scale Transform (IMST) is applied to create the fused image.

2.1 Image Fusion Using the Weighted Average

The fusion method based on the weighted average is a pixel level method that using weights assigned to each original image, the weight may be fixed or variable based on specific applications; commonly using the sharpness analysis to assigns a higher weight to the sharpest pixels in the input images [10]. The weights for each source image are defined by two arrays W_1 and W_2, where $0 \leq W_1, W_2 \leq 1$ and $W_1(x, y) + W_2(x, y) = 1$, a resulting image is given by the equation 1.

$$I(x, y) = W_1(x, y)I_1(x, y) + W_2(x, y)I_2(x, y) \tag{1}$$

To calculate the weight array is used the information from the image edges obtained by applying high-pass filters which reflect the abrupt changes in the intensities of the pixels with respect to its environment (edges).

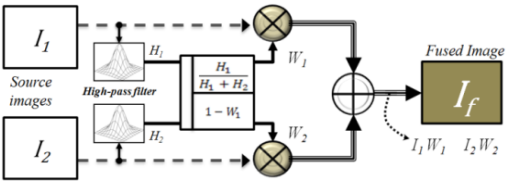

Fig. 2. Illustration of the weighted average fusion method

To obtain the related frequencies components of the edges in the images, was used a high-pass filter, is a Gaussian 3x3 convolution kernel that uses the concept of the second derivative defined by equation 2. Thus if H_1 contains the edges information of the picture I_1 and H_2 to the image I2, in both cases by the application of predefined kernel. The weights can be obtained as shown in Figure 2.

$$H(x,y) = |h * I(x,y)| \rightarrow h = \begin{bmatrix} -1 & -1 & -1 \\ -1 & 8 & -1 \\ -1 & -1 & -1 \end{bmatrix} \quad (2)$$

2.2 Image Fusion Using Principal Component Analysis

The fusion method based on the principal component analysis [11] is a straightforward way to build a fused image as a weighted superposition of several input images. The optimal weighting coefficients, with respect to information content, can be determined by a principal component analysis of all input intensities. By performing a PCA of the covariance matrix of input intensities, the weightings for each input image are obtained from the eigenvector corresponding to the largest eigen-value. Figure 3 shows the basic fusion scheme, where two images I_1 *and* I_2 are fused to obtain a resultant image I_f given by equation 3, W_1 *y* W_2 are the weights coefficients.

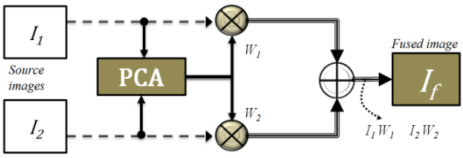

Fig. 3. PCA operation to fuse two images

$$I_f(x,y) = W_1(x,y)I_1(x,y) + W_2(x,y)I_2(x,y) \quad (3)$$

The weights for each source image are obtained from the eigenvector corresponding to the largest eigen-value of the covariance matrix of each source. Arrange source images in two-column vector.

- Organize the data, let S be the resulting column vector.
- Compute empirical mean (M_e) along each column.
- Subtract M_e from each column of S, the resulting is a matrix X.
- Find the covariance matrix C of matrix X.
- Compute the eigenvectors V and eigen-value and sort them by decreasing eigen-value.
- Consider first column which correspond to larger eigen-value to compute normalized component W_1 *and* W_2.

2.3 Laplacian Pyramid Image Fusion

Laplacian pyramid of an image is a set of band-pass images, in which each is a band-pass filtered copy of its predecessor [12]. Band-pass copies can be obtained by

calculating the difference between low-pass (Gaussian filter) images at successive levels of a Gaussian pyramid. In Laplacian fusion approach the Laplacian pyramids for input images are used. A strength measure is used to decide from which source what pixels contribute at each specific sample location. Given an image I, the first level of its Gaussian pyramid is defined as a copy of the original image and the k-th level is defined by the equation 4 and the k-th level of the Laplacian pyramid is defined by the equation 5, where $\downarrow 2$ and $\uparrow 2$ denotes a down-sampling and up-sampling at a factor of 2, w represent a 5x5 low-pass filter kernel

$$G_k(x,y) = [w * G_{k-1}(x,y)]_{\downarrow 2} \tag{4}$$

$$\tilde{L}_k(x,y) = G_k(x,y) - 4w * [G_{k-1}(x,y)]_{\uparrow 2} \rightarrow w = \frac{1}{256}\begin{bmatrix} 1 & 4 & 6 & 4 & 1 \\ 4 & 16 & 24 & 16 & 4 \\ 6 & 24 & 36 & 24 & 6 \\ 4 & 16 & 24 & 16 & 4 \\ 1 & 4 & 6 & 4 & 1 \end{bmatrix} \tag{5}$$

To reconstruct the original image I from both pyramids (Laplacian and Gaussian), is used equation 6. The fusion of the low-pass coefficients involves blending all the Gaussian pyramid coefficients; the fusion of the high-pass coefficients involves blending only the level of the Laplacian pyramid. Zhang and Blum [13] proposed a combination method, where the coefficients are considered separately; the low pass coefficients are fused using the arithmetic mean and the high pass coefficients according with the biggest absolute value (see equations 7 and 8).

$$\hat{G}_k(x,y) = \tilde{L}_k(x,y) + 4w * [\hat{G}_{k+1}(x,y)]_{\uparrow 2} \tag{6}$$

$$G_k^C(x,y) = \frac{G_k^A(x,y) + G_k^B(x,y)}{2} \tag{7}$$

$$\tilde{L}_k^C(x,y) = \begin{cases} \tilde{L}_k^A(x,y) & if \quad \left|\tilde{L}_k^A(x,y)\right| > \left|\tilde{L}_k^B(x,y)\right| \\ \tilde{L}_k^B(x,y) & otherwise \end{cases} \tag{8}$$

2.4 Contrast Pyramid Image Fusion

The composite images produced by this scheme preserve those details from the input images that are most relevant to visual perception [14].The essential problem in fusion images for visual display is pattern conservation: important details of the component images must be preserved in the resulting fused image, while the fusion process must not introduce spurious pattern elements that could interfere with succeeding analysis. Contrast itself is defined as the ratio of the difference between luminance at a certain location in the image plane and local background luminance to the local background luminance. Luminance is defined as the quantitative measure of brightness and is the amount of visible light energy leaving a point on a surface in a given direction. The construction of the Contrast pyramid is similar to the construction of the Laplacian pyramid. First a Gaussian pyramid is constructed by equation 9, which describes the k-th level of the pyramid and the reconstruction is defined by Equation 10. The coefficients fusion methodology employs a method similar to the Laplacian pyramid (see equation 7). However, to fuse the Laplacian coefficients are used the absolute maximum criterion described by Equation 11.

$$R_k(x,y) = G_k(x,y)/4w * [G_{k-1}(x,y)]_{\uparrow 2} \tag{9}$$

$$\hat{G}_k(x,y) = R_k(x,y) * 4w * [\hat{G}_{k+1}(x,y)]_{\uparrow 2} \tag{10}$$

$$R_k^C(x,y) = \begin{cases} R_k^A(x,y) & if \quad \left|R_k^A(x,y) - 1\right| > \left|R_k^B(x,y) - 1\right| \\ R_k^B(x,y) & otherwise \end{cases} \tag{11}$$

2.5 Gradient Pyramid Image Fusion

The gradient pyramid is emerging as a variation to the Laplacian pyramid. A gradient pyramid is obtained by applying a set of 4 directional gradient filters (horizontal, vertical and 2 diagonal) to the Gaussian pyramid at each level. At each level, these 4 directional gradient pyramids are combined together to obtain a combined gradient pyramid that is similar to a Laplacian pyramid. The gradient pyramid fusion is therefore the same as the fusion using Laplacian pyramid except replacing the Laplacian pyramid with the combined gradient. The k-th level with l orientation of the gradient pyramid is defined by equation 12. G_k is the k-th level of the Gaussian pyramid, d_l is the gradient filter for the l orientation and w is a Gaussian filter kernel described by equation 12, the gradient filters are given by equations (13-16).

$$D_{k,l}(x,y) = d_l * [G_k(x,y) + \dot{w}G_k(x,y)] \rightarrow \dot{w} = \frac{1}{16}\begin{bmatrix} 1 & 2 & 1 \\ 2 & 4 & 2 \\ 1 & 2 & 1 \end{bmatrix} \tag{12}$$

$$d_1 = [1 \quad -1], \qquad d_2 = \frac{1}{\sqrt{2}}\begin{bmatrix} 0 & -1 \\ 1 & 0 \end{bmatrix}, \qquad d_3 = \begin{bmatrix} -1 \\ 1 \end{bmatrix}, \qquad d_4 = \frac{1}{\sqrt{2}}\begin{bmatrix} -1 & 0 \\ 0 & 1 \end{bmatrix} \tag{13-16}$$

To reconstruct the image from the gradient pyramids is used equation 17. The fusion of coefficients involves the same methodology of the Laplacian pyramid.

$$\tilde{L}_k(x,y) = [1+w] * \sum_{l=1}^{4} (-\frac{1}{8} d_l * D_{k,l}(x,y)) \tag{17}$$

2.6 FSD Pyramid Image Fusion

FSD (filter, subtract, decimate) pyramid technique [15], is a variation of the Laplacian fusion. In Laplacian pyramid, the difference image L_k at level k is obtained by subtracting an image up-sampled and then low-pass filtered at level $k+1$ from the Gaussian image G_k at level k, while in FSD pyramid, this difference image is obtained directly from the Gaussian image G_k at level k subtracted by the low-pass filtered image of G_k as a result, FSD pyramid fusion method is computationally more efficient than the Laplacian pyramid method by skipping an up-sampling step.

$$L_k(x,y) = G_k(x,y) - w * G_k(x,y) \tag{18}$$

$$\hat{G}_k(x,y) = L_k(x,y) + w * (L_k(x,y) + \left[4\hat{G}_{k+1}(x,y)\right]_{\uparrow 2}) \tag{19}$$

The calculation of the k-th level of the Laplacian pyramid is computationally more efficient (see equation 18), however this variation restricts to use the equation 6. Thus it is necessary to define a different reconstruction formulation given by equation 19. The coefficients fusion uses the same methodology of the Laplacian pyramid.

2.7 Image Fusion Based on Wavelet Decomposition

The Wavelet transform decomposes an image into various sub images based on local frequency content [16]. The discrete Wavelet transform (DWT) coefficients are computed by using a series of low pass filter L[k], high pass filters H[k] and down samplers across both rows and columns. The results are the wavelet coefficient the next scale. The filter bank approach to calculate two dimensional dyadic DWT is shown in figure 4. The wavelet coefficients are of smaller spatial resolution as they go from finer scale to coarser scale. The wavelet representation has the advantage of not generating redundant information since functions are orthogonal, thus original image can be reconstructed from the wavelet decomposition of an inverse algorithm.

According with equations (20-23), we can define the k-th level of the pyramid of Wavelets, where $(1 \downarrow 2)$ is a down-sampling to remove half of the rows of the image and $(2 \downarrow 1)$ to remove half of the columns of the image. The pyramid is constructed by applying this decomposition recursively on approximation coefficients. To reconstruct the image, we must apply the inverse transformations.

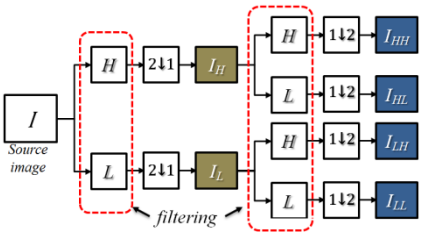

Fig. 4. Two-dimensional orthogonal Wavelet fusion

$$LL_k(x,y) = [w_L * [w_L * I_k(x,y)]_{2\downarrow1}]_{1\downarrow2} | W_L = \frac{1}{\sqrt{2}}[1 \quad 1] \tag{20}$$

$$LH_k(x,y) = [w_H * [w_L * I_k(x,y)]_{2\downarrow1}]_{1\downarrow2} | W_H = \frac{1}{\sqrt{2}}[-1 \quad 1] \tag{21}$$

$$HL_k(x,y) = [w_L * [w_H * I_k(x,y)]_{2\downarrow1}]_{1\downarrow2} | W_L = \frac{1}{\sqrt{2}}[1 \quad 1] \tag{22}$$

$$HH_k(x,y) = [w_L * [w_H * I_k(x,y)]_{2\downarrow1}]_{1\downarrow2} | W_H = \frac{1}{\sqrt{2}}[-1 \quad 1] \tag{23}$$

Finally, the reconstructed image is obtained from Equation 24.

$$\hat{I} = LL_k^{-1}(x,y) + LH_k^{-1}(x,y) + HL_k^{-1}(x,y) + HH_k^{-1}(x,y) \tag{24}$$

3 Experimental Results

3.1 Database

In order to evaluate the performance of the fusion methods, were handled a test set with 120 iris images from different videos of the Multiple Biometrics Grand Challenge “MBGC.v2” [17] database. All videos were acquired using an LG2200 camera with near-infrared illumination of the eye, some features: MPEG-4 format and the size for each frame in the video has 480 rows and 640 columns in 8 bits-grayscale space. The MBGC.v2 database presents noise factors, especially those relative to reflections, contrast, luminosity, eyelid and eyelash iris obstruction and focus characteristics. These facts make it the most appropriate to study the iris recognition system for uncontrolled environments. The test set is composed by 10 videos from 10 different people, for each video were randomly selected 10 images, analyzing and verifying that each image met the minimum quality parameters and segmentation rates exposed by Colores et al. [18]. In addition, we selected two reference images from each video for biometric comparison purposes, a reference image called "Reference 1" was chosen from the video based on the higher energy criterion [18], and the reference image called "Reference 2" was chosen based on the best subjective quality perceived. Each image in the set of test was segmented and normalized using the algorithms for iris recognition of Libor Masek [19], obtaining for each image a normalized template; this template contains only the texture information of the iris region. As mentioned in the first section, the recognition process is based on the value of the Hamming distance; this value reflects the correlation between two digital biometric templates. The digital biometric template is obtained from the normalized template by the encoding stage of an iris recognition system. In this sense, the Hamming distance will have a small value if digital biometric templates generated from the same iris (*comparison Intra-class*) are compared, or otherwise will have a value close to 1 (*comparison Inter-class*). In this paper, we are focused on improving the recognition by reducing the Hamming distance, this serves to reduce the chances of a false match. Hence, all possible Intra-class comparisons were performed on the test set, 100 comparisons for each reference image. In Figure 5, are illustrated Hamming distance values for different Intra-class comparisons, it can be seen that correlation values show a similar behavior in the two reference images, with average values of 0.2871 and 0.2863 for the image reference 1 and 2 respectively.

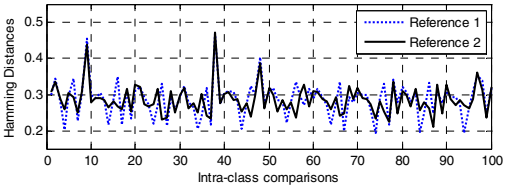

Fig. 5. Hamming distance values obtained from intra-class comparisons

3.2 Comparison of Image Fusion Schemes

The experimental analysis involves fusing pairs of normalized templates. Figure 6 illustrates the fusing process for normalized templates for each video. We calculated a total of 100 new fusioned normalized templates for each analyzed fusion method.

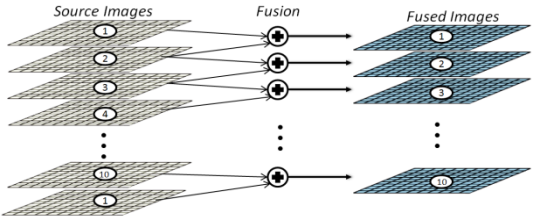

Fig. 6. Fusing process for normalized templates for each video

We implemented seven fusion methods described in section 2, intra-class comparisons were performed again with the 100 new digital biometric templates fused by each method, and the purpose was to determine the method that enhances the intra-class correlation values, as this could increase recognition rates by reducing the values of Hamming distances. Figure 7 shows the percentage of the experiments which had an improvement in the reduction of the Hamming distance for each method tested.

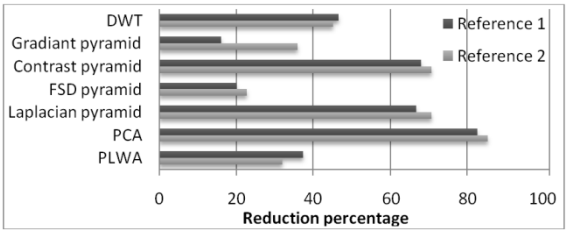

Fig. 7. Reduction percentage of Hamming distance for experiments with fusion methods

The fusion method based on principal component analysis PCA has the best performance compared to other methods; this does reduce the Hamming distance values in approximately 83% of the experiments. In Figures 8-9, are shown the variation between the Hamming distance values obtained from the intra-class comparison before and after to deploy the FSD and Gradient pyramid fusion methods. It can be appreciated that in these fusion methods, the majority of intra-class comparisons increased the Hamming distance values. Moreover, the fusion methods able to improve the correlation values in a high percentage of intra-class comparisons are performed by PCA, Laplacian pyramid and Gradient pyramid.

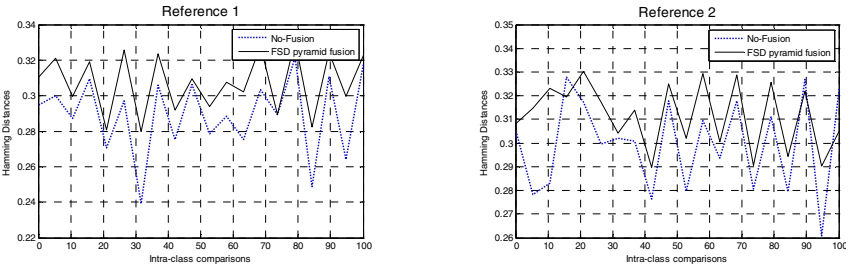

Fig. 8. Hamming distance values. After to deploy the FSD pyramid image fusion.

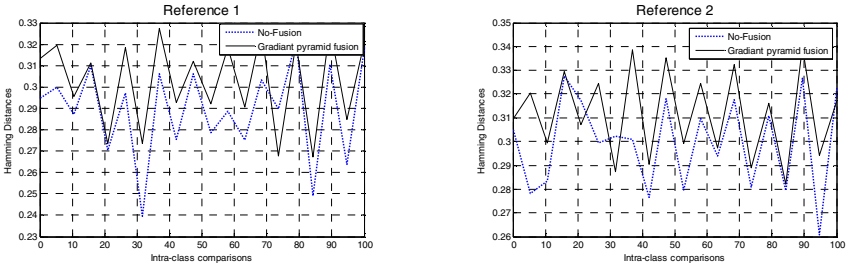

Fig. 9. Hamming distance values. After to deploy the Gradient pyramid image fusion.

Figure 10, shown the reduction in the Hamming distance values which were obtained by implementing the PCA fusion method. This method achieve the better percentage reduction in the experiments, reduces an average Hamming distance value in 0.015. Laplacian pyramid fusion methods and Contrast pyramid fusion method only reduce an average Hamming distance value at 0.0102. It is remarkable reduction in value of the Hamming distance at implement the PCA fusion method, which can project a possible reduction in the recognition error rates when implemented as a new module in a biometric system for uncontrolled environments.

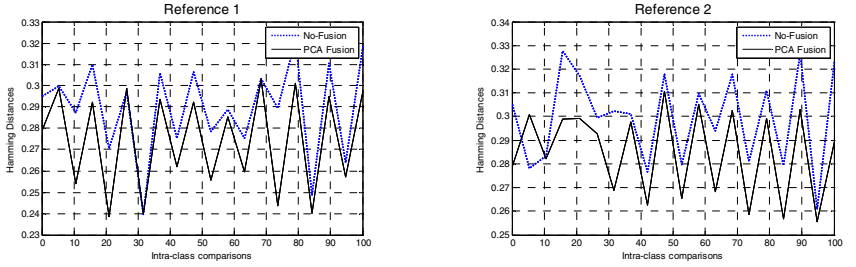

Fig. 10. Hamming distance values. After to deploy the PCA image fusion.

4 Conclusions

This paper proposes to exploit the biometric information from video-iris acquired under non-cooperative scheme, creating a fusioned normalized template through an

image fusion technique. The performances of seven image fusion methods are evaluated. The experimental results show that the PCA method presents the best performance to improve recognition values according to the Hamming distances in 83% of the experiments. In PCA, it is assumed that the information is carried in the variance of the features that is equivalent to walking around the data to see from which one gets the best information. In our opinion, the underlying reason is that PCA is more suitable to obtain the weights for iris images fusion, it's that analysis is based on small samples statistically independent (columns) of the source images data, resulting in a weights matrix more accurately. Thus, the results suggest that adding a fusion module to the architecture of the non-cooperative iris recognition, it could increase the system performance. Therefore, we can conclude that our proposal can be integrated as an optimization to the system developed by Colors et al [18], for an application of iris recognition in uncontrolled environments.

Acknowledgment. This research was supported by grant SIP 2013 from Instituto Politécnico Nacional.

References

1. Daugman, J.: How Iris Recognition Works. IEEE Transactions on Circuits and Systems for Video Technology 14, 21–30 (2004)
2. Wildes, R.: Iris Recognition: An Emerging Biometric Technology. Proceedings of the IEEE 85(9), 1348–1363 (1997)
3. Gamassi, M., Lazzaroni, M., Misino, M., Piuri, V.: Quality assessment of biometric systems: a comprehensive perspective based on accuracy and performance measurement. IEEE Trans. Instrum. Meas. 54, 1489–1496 (2005)
4. Vatsa, M., Singh, R., Gupta, P.: Comparison of Iris Recognition. In: International Conference on Intelligent Sensing and Information Processing, pp. 354–358 (2004)
5. Hollingsworth, K., Peters, T., Bowyer, K.: Iris recognition using signal-level fusion of frames from video. IEEE Transa. Inform. Forensics Secur. 4(4), 837–848 (2009)
6. Lee, Y., Phillips, P., Michaels, R.: An automated video-based system for iris recognition. In: Proc. Int. Conf. Biom., pp. 1–8 (2009)
7. Colores-Vargas, J., García, M., Ramírez, A., García, M., Nakano, M., Perez, H.: Iris recognition system based on video for unconstrained environments. Scientific Research and Essays 7(35), 3114–3127 (2012)
8. Jillela, R., Ross, A., Flynn, P.: Information Fusion in Low-resolution Iris Videos Using Principal Components Transform. In: Proceedings of IEEE Workshop on Applications of Computer Vision (WACV), Kona, USA (January 2011)
9. Mitchell, H., Singh, R., Gupta, P.: Multifocus Method for Controlling Depth of Field. Grafica Obscura (1994)
10. Haeberli, P., Singh, R., Gupta, P.: Image Fusion: Theories, Techniques and Applications. Springer, Heidelberg 2010 (2004)
11. Pajares, G., De la Cruz, J.: Visión por Computador: Imágenes Digitales y Aplicaciones. RA-MA, Madrid (2001)
12. Burt, P., Kolczynski, R.: Enhanced image capture through fusion. In: Proc. Fourth Int. Conf. on Computer Vision, pp. 173–182 (1993)

13. Zhang, Z., Blum, R.: A categorization of Multiscale-Decomposition-Based Image Fusion Schemes with a Performance Study for a Digital Camera Application. Proc. IEEE 87(8), 1315–1326 (1999)
14. Toet, A., van Ruyven, J., Valeton, J.: Merging termal and visual images by a contrast pyramid. Optical Engineering 28(7), 789–792 (1989)
15. Anderson, H.: A filter-subtract-decimate hierarchical pyramid signal analyzing and synthesizing technique. U.S. Patent 4.718 104 (1987)
16. Mallat, S.: A theory for multiresolution signal decomposition: the wavelet representation. IEEE Trans. Pattern Anal. Mach. Intell. 11, 674–693 (1989)
17. Multiple Biometric Grand Challenge, http://face.nist.gov/mbgc/
18. Colores-Vargas, J.M., García-Vázquez, M.S., Ramírez-Acosta, A.A.: Measurement of defocus level in iris images using convolution kernel method. In: Martínez-Trinidad, J.F., Carrasco-Ochoa, J.A., Kittler, J. (eds.) MCPR 2010. LNCS, vol. 6256, pp. 125–133. Springer, Heidelberg (2010)
19. Masek, L.: Recognition of human iris patterns for biometric identification. Master's thesis, University of Western Australia (2003)